Novel Estimation Framework for Short-Circuit Current Contribution of Type IV Wind Turbines at Transient and Steady-State of the Faults

Gabriel M. G. Guerreiro[1,2*], Ramon Abritta[3], Kaio V. Vilerá[2,4], Ranjan Sharma[1], Frank Martin[1], Guangya Yang[2]
[1] Siemens Gamesa Renewable Energy A/S, Denmark, {gabriel.gomes*, ranjan.sharma, frank.martin}@siemensgamesa.com
[2] Technical University of Denmark (DTU), Denmark, {gamgu*, kavil, gyyan}@dtu.dk
[3] Norwegian University of Science and Technology (NTNU), Norway, {ramon.a.santos}@ntnu.no
[4] Typhoon HiL, Serbia, {kaio.vilera}@typhoon-hil.com

***Abstract*—Given the increasing penetration of converter-interfaced resources in power systems, properly estimating the short-circuit current (SCC) contribution in large networks has become a growing challenge and necessity to ensure the security and stability of the systems and assets. This paper presents two novel methods to estimate the SCC contribution of type IV wind turbines at both the transient and steady-state stages of unbalanced and balanced faults: 1) a machine learning-based method trained with electromagnetic transient (EMT) simulations and capable of estimating some of the initial peak and transient current magnitudes; 2) an analytical approach to estimate the steady-state SCC based on the voltage and grid code dependency of the converter during the fault. The methods are coupled into a single framework and compared to field-validated EMT models of a real turbine. The results show that the majority of the estimated currents in the transient stages present errors below 5%. In steady-state, the errors are not greater than 1.21%. Given the complexity of the problem, these margins may be deemed acceptable for short-circuit studies.**

***Index Terms*—Short-Circuit Current, Analytical Modelling, Estimation Methods, Machine Learning, type IV Wind Turbines**

I. Introduction

Correct estimation of the short-circuit current (SCC) contribution of different power sources is crucial in preventing blackouts, maloperation of relays, and equipment damage. To prevent those, short-circuit studies utilizing different tools are applied to equipment design and protection coordination. According to standards and guidelines, the maximum SCC contribution is used to define the rating of equipment regarding mechanical and thermal stresses, while the minimum is used for the selection of system protection [1, 2]. Furthermore, the levels of SCC and equilibrium points during faults are becoming important to define the stability and control strategies for the modern system in highly-penetrated converter systems.

Current practice usually neglects or simplifies the contribution from Inverter-Based Resources (IBRs). In general, short-circuit studies follow standards such as IEC 60909-0 Ed. 2 and ANSI / IEEE C37. For instance, during the steady-state stage of the fault, IEC 60909-0 Ed. 2 represents the contributions of type IV wind turbine generators (WTGs) as current sources fixed at around 1.1 to 1.5 p.u., depending on the converter capability [2]. However, as the current of a type IV WTG behaves in a more complex way during a fault, the standards usually fail to state the dependency on many factors [3].

Recent work based on standards was performed to calculate the SCC contribution with general assumptions for modeling IBRs as static current sources [4]. Aside from standard-related works, a phasor-model-based approach was used in [5, 6] to model the SCC contribution at steady-state of type IV WTGs as a voltage-dependent current source with an algorithm that can achieve similar results as an EMT simulation. Furthermore, methods presented in papers such as [7] estimate contributions from electronically coupled distributed energy resources. However, the utilized formulation relates to doubly-fed induction generators (type 3), as presented in [8], and should not be generalized to the broad scope of resources based on power electronics. Finally, systematic reviews of the short-circuit characteristics of IBRs were recently done in[3].

Despite recent work on estimating SCC during steady-state, there are still important factors to be further explored for type IV WTGs. For example, comparison with field-validated EMT models, evaluation of active current injection, types of voltage dependency and other grid-code-dependent parameters, and behavior during unbalanced faults. Furthermore, not much work has attempted to estimate currents during the transient stages of the fault in type IV WTGs. In this sense, this paper contributes to three different aspects: 1) A novel analytical approach that estimates the steady-state current contribution; 2) A novel machine-learning-based approach for estimating the peak current; 3) Discussions on different challenges and new standardization required for short circuit current estimation.

The rest of the paper is structured as follows. Section II provides an overview of the fault stages in an industrial large-scale type IV WTG. In addition, it gives definitions of the control, models, and methodology. The industrial model is based on Siemens Gamesa's Direct Drive (DD) wind turbine. Section III introduces the methodology for the analytical

Submitted to the 23rd Power Systems Computation Conference (PSCC 2024).

estimation of the steady-state during-fault current. Section IV presents the machine-learning-based approach for estimating the peak current during the fault. Section V concludes the work by discussing the proposed methods. The comprehensive methodology developed in this paper can be utilized to estimate the SCC of type IV WTGs accurately for equipment and protection design. It does not need any proprietary knowledge of the black-box control as in root-mean-square (RMS) or EMT simulation. Furthermore, it can be used for early design or long-term planning of inverter-dominated power systems.

II. Definitions of Three Stages of the Fault, Control Systems and Models

In this section, a short explanation of the converter control system adopted by industrial wind turbines is given, followed by a description of the model setup, the validation procedure, and the data acquisition process.

A. Three Stages of the Fault

Fig. 1 displays how the type IV WTG typically responds to a specific power system fault. Where currents I^+_{react}, I^-_{react}, I^+_{act}, and I^-_{act} are the positive and negative sequence reactive and active currents, respectively. In real converter setups, changes in feedback signals always imply a time delay between the occurrence of a fault and the corresponding reaction of the converter control system. This delay also encompasses the time required for the system to recognize the fault. This can be seen from the currents' behavior shown in Fig. 1.I^+_{react} and I^-_{react} start to change after a certain delay subsequent to the occurrence of the fault, and the control acts to provide reactive power support to mitigate the fault's impact. This response is not instantaneous due to control bandwidths, measurement methods, filtering, and communication delays inherent in the system. The EMT simulation, validated with real measurements, includes these aspects. As a result, it is possible to define three distinct stages of a fault for a type IV WTG: the sub-transient, the transient, and the steady state.

At the beginning of the sub-transient stage of a fault in a type IV WTG, the control has not yet identified the fault and has not started the transition to fault-ride-through (FRT) control mode. At this stage, the currents can rise to values higher than the in-fault steady-state magnitudes and present sequence component characteristics that do not correspond to the FRT current priority. At the transient stage, the control starts to react to the changes of the fault and identifies the FRT event. The currents start to be controlled and brought back to desired values, which are usually limited to around 1.1 p.u. During both transient stages, the behavior of the current is very complex to determine analytically, as it is influenced by many factors [3]. Therefore, to estimate peak and maximum currents taking into account all the parameters involved in the initial response of the turbine, a machine learning-based methodology was developed and explained in Section IV.

Finally, at the steady-state stage, which usually starts from 50 ms, the values have either fully or almost fully settled to the desired in-fault injection depending on the grid code. The behavior of the converter can be modeled as a voltage- and grid-code-dependent current source. This part can be estimated analytically, as presented in Section III.

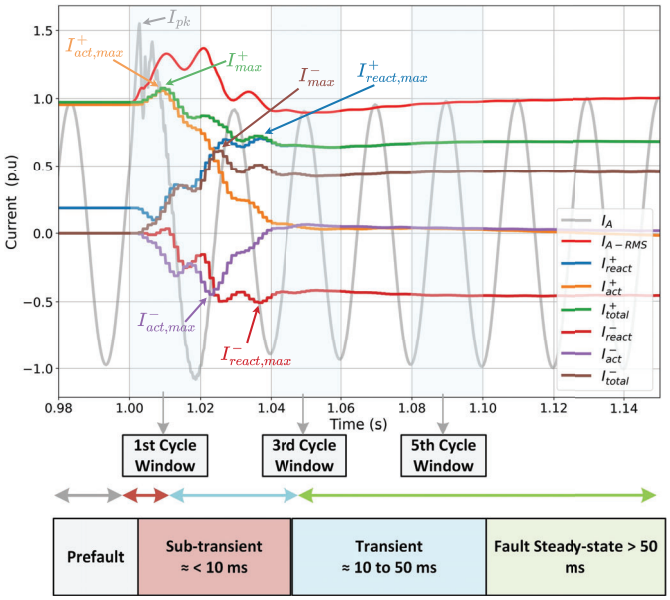

Fig. 1. Data acquisition example for a two-phase fault with priority given to both positive and negative sequence currents.

B. Grid-Following and Fault Ride-Through Control Systems

Fig. 2 shows a simplified view of the grid-following control utilized in this study. The voltages and currents used for the feedback loop of the control are measured after the filter and reactor. A phase-locked loop (PLL) is used to synchronize with the systems' frequency and provide the phase angle references for the ABC-dq transformations. The outer voltage/power control loop receives the power and/or voltage references from the wind power plant (WPP) controller, subsequently computing the reference currents within the dq-frame to be transmitted to the current control. This process relies primarily on the main inputs to the individual wind turbine, namely the power and voltage set points, which are instrumental in guiding the control mechanism under normal operation.

During a fault ride-through (FRT) event, the FRT control takes over and defines the dq-current references for the inner current control, based on the different pre-fault and during-fault measurements as well as the specific grid code requirements. FRT is defined as the capability of an electrical equipment or system to endure and maintain stable operation during a transient deviation in voltage, typically an under-voltage condition. While sustaining the fault, many grid codes request power stations to perform voltage support in the form of reactive current injection. The injected current can either be composed only by the positive sequence or by both positive and negative sequences. The total current is then restricted to the equipment's limitation and passed to the inner current control loop which produces the voltage references for the pulse-width modulator (PWM). It is important to mention that,

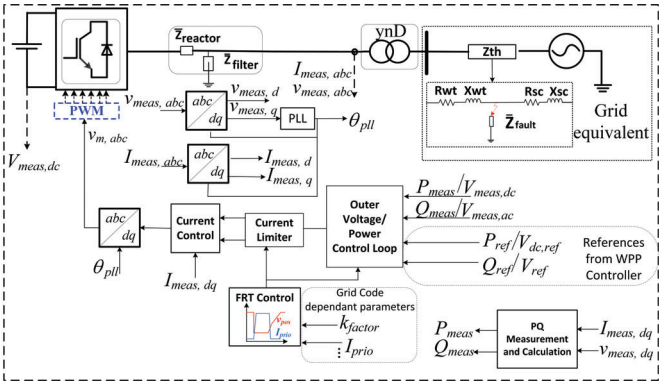

Fig. 2. Grid-side grid-following control topology [3].

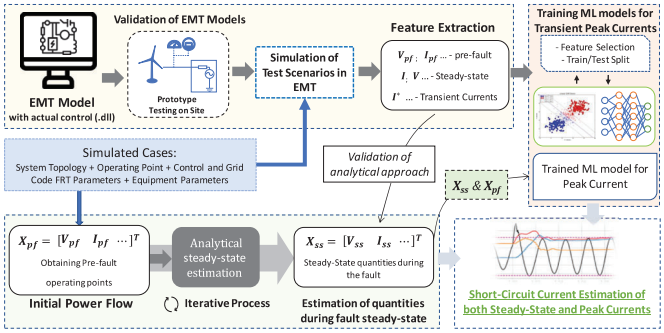

Fig. 3. Flowchart of the combined methods to estimate the current contribution at the transient and steady-state stages of unbalanced and balanced faults.

for this paper, the FRT control is activated based on a settable parameter that represents the voltage drop below a certain threshold ranging typically from 0.85 to 0.95 p.u. For the case of this paper, the value of 0.9 is used in both grid codes.

C. Model Definition and Validation

The industrial EMT model of the type IV WTG used in this paper is validated against real-site measurements for FRTs and is developed in PSCAD™. The modeled mechanical system consists of the aerodynamic and shaft models. The electrical system includes the permanent magnet synchronous generator, full converter, DC link, grid-side converter reactor, filter, WTG transformer with saturation and frequency-dependent impedance, and measurement ports. Finally, the control system includes the WTG level controller with reduced-order functionalities deemed necessary for EMT-type simulations and the converter controller which is responsible for controlling the generator and grid side converters as well as the DC link. The actual full-order code of the converter control, with the source code embedded as a *.dll* (dynamic link library), and protection, including turbine and converter level protection, are also implemented in the model.

Prior to carrying out extensive simulations for this paper, the model was validated against real-site measurements for FRTs, according to different grid codes and standards such as IEC 61400-21-1 [9]. In addition to performing tests and validation on prototype turbines in the field, the industry is also making progress in testing individual parts and subsystems, along with real-time solutions that involve both hardware and software integration [10].

D. Simulated System and Data Acquisition

A conventional single-turbine system, interfaced with a Thevenin equivalent circuit, serves as the experimental model. Before the introduction of the fault in each simulation, the WTG was allowed to initialize and attain a steady-state condition. A set of EMT simulations was performed, using a time step lower than 10 μs and a sampling rate of 5 kHz to save the data. Posterior to simulation, the data was pre-processed to be used for validation of the steady-state method and training/testing of the machine learning method. All sequence components were calculated using full-cycle windows (i.e. 20 ms for 50 Hz) and a sampling rate of 2 kHz. All faults were simulated for more than 150 ms so that a steady-state fault condition was achieved. Measurements of steady-state currents and voltages started 100 ms after the fault occurrence. Then, they were averaged for the rest of the fault period.

E. Proposed Framework: Methods for Estimating Steady-State and Peak Currents

Two novel estimation methods are presented in Sections III and IV, one for the steady state and another for the transient stage of the fault, as seen in Fig. 3. The validated EMT model is used to obtain the signatures for training the machine learning (ML) models and to validate the analytical approach. After obtaining reliable models, the entire solution can be used together, where analytical steady-state estimations can also feed the training ML models so that peak currents can be estimated. The methodologies will be explained in the following sections.

III. Steady-State Current Analytical Estimation

This section proposes an analytical approach to estimate steady-state SCC contributions of type 4 WTGs during balanced faults. Today's industrial context mostly relies on standards such as IEC 60909-0:2016, which models type IV WTGs as fixed current sources during a fault. However, although WTGs behave as current sources in such scenarios, the reactive current magnitude (I_r) depends on the residual voltage (V_{res}^+) at the WTG terminals, as in Eq. 1. In this example, the priority is given only to the positive sequence. K_{factor} is the converter's current control proportional gain; V_C is a voltage quantity dependent on the grid code (GC); I_r^+ is the positive sequence reactive current that the converter injects based on V_C and V_{res}^+; $I_{r,lim}^+$ is the FRT limit for the positive sequence reactive current injection; $I_{r,pf}^+$ is the reactive component of the pre-fault WTG current; and D_{band} is the considered deadband for the voltage difference.

$$I_r = \begin{cases} I_r^+ = K_{factor}\left(|V_C| - |V_{res}^+| - D_{band}\right) + I_{r,pf}^+ \\ I_r^- = 0 \\ I_r^+ + I_r^- \leq I_{r,lim}^+ \end{cases} \quad (1)$$

This paper addresses the following grid codes:

- GC1 - V_C is the WTG nominal voltage (1 p.u.) and neither the deadband nor pre-fault reactive current is included in the calculation of the current injection during a fault, as in (2). The GC1 is based on the EON GmbH Grid Code, High and Extra High Voltage [11];
- GC2 - V_C is the WTG pre-fault voltage (V_{pf}) minus a deadband equal to 0.1. Furthermore, the reactive component of the pre-fault WTG current ($I^+_{r,pf}$) is added to the right-hand side of the I^+_r calculation, as in (3). The GC2 is based on the Ordinance on System Services by Wind Energy Plants (SDLWindV) [12].

$$\text{GC1} : I^+_r = K_{factor} \cdot \left(1 - |V^+_{res}|\right) \tag{2}$$

$$\text{GC2} : I^+_r = K_{factor} \cdot \left(|V_{pf}| - |V^+_{res}| - 0.1\right) + I^+_{r,pf} \tag{3}$$

Several other grid codes could be considered, especially codes where negative sequence reactive current injection during unbalanced faults is required. Nonetheless, grid codes GC1 and GC2 are deemed to represent well the two main variants that affect three-phase faults, which do not require negative sequence injection.

The proposed analytical approach has three stages. First, a traditional power flow obtains the pre-fault conditions. Second, a power flow adaptation handles the current source behavior of the WTG during faults. Finally, an iterative strategy obtains the fault steady-state current according to (1).

A. Newton-Raphson Power flow adaptation

In general, power flow formulations model buses as PQ, PV, and Vθ. By bringing active and reactive power mismatches to zero, an iterative process determines the voltages and angles of PQ buses and the angles of PV buses. In this paper, a WTG can be modeled as a PV bus during steady-state normal operation since voltage and active power are used as references for the control. However, during a fault, the WTG's control assumes a current source behavior that cannot be modeled as a PV or as a PQ bus, since the WTG does not follow the power and voltage references sent by the plant controller.

Therefore, the standard Newton-Raphson formulation is adapted by: (i) replacing the WTG PV bus with a PQ bus with null loads, hence adding one reactive power mismatch equation; (ii) including a current source linked to the new PQ bus via the reactor impedance (Z_r); (iii) adding two new equations related to active and reactive current mismatches. Fig. 4 exhibits the system models pre and during the fault, in which Z_{fi}, Z_b, Z_t, Z_{th}, Z_{fa} are the filter, busbar, transformer, grid Thevenin, and fault impedances, respectively; f_{loc} and f^*_{loc} are the fault location ($\in [0,1]$) and its complement ($1 - f_{loc}$); I_{ref} is the reference current phasor.

As an important remark, the pre-fault model does not include the reactor since the WTG voltage reference is after the mentioned component. However, during the fault, the WTG converter "sees" the fault from the perspective of the current source in Fig. 4. Thus, including the reactor implies a more accurate representation.

When adding a current source to the WTG model, the power flow calculation starts with specified/reference values for the active (I^a_{ref}) and reactive (I^r_{ref}) currents. This is analogous to the procedure of providing active power references to PQ and PV buses, and reactive power references to PQ buses. In the adapted power flow, the method starts with initial voltage and angle guesses for PQ and current buses, and angle guesses for PV buses. Then, the algorithm defines the P, Q, and current mismatches according to the references and to the calculated quantities based on the guesses. From the I^r_{ref} guess, (4) describes I^a_{ref}, in which I_{max} is the maximum magnitude of the current phasor. It is noteworthy that the proposed approach always utilizes $I^+_{r,lim}$ as the initial guess for I^r_{ref}.

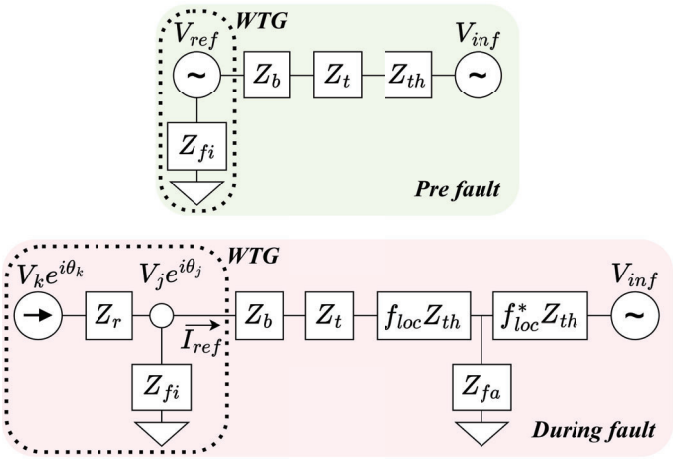

Fig. 4. Power flow model at pre- and during-fault conditions.

$$I^a_{ref} = \sqrt{(I_{max})^2 - (I^r_{ref})^2} \tag{4}$$

In Fig. 4, the WTG links to a PQ bus between Z_b and Z_t. The current in this path is the one injected by the WTG, so it is chosen as the reference. Equation (5) describes the current calculation. Upon expansion of (5), (6) and (7) describe the active (I^a_{calc}) and reactive (I^r_{calc}) currents calculated from the initial guesses. By obtaining the partial derivatives of the current mismatches, (8), relative to the variables of the problem (voltages of PQ and current buses; angles of PQ, PV, and current buses), one can compute the Jacobian.

$$I_{calc} = \frac{V_k e^{i\theta_k} - V_j e^{i\theta_j}}{Z_r} - \frac{V_j e^{i\theta_j}}{Z_{fi}} \tag{5}$$

$$I^a_{calc} = \frac{\Psi R_r + \Phi X_r}{R_r^2 + X_r^2} - V_j \frac{R_{fi}\cos\theta_j + X_{fi}\sin\theta_j}{R_{fi}^2 + X_{fi}^2} \tag{6}$$

$$I^r_{calc} = \frac{\Phi R_r - \Psi X_r}{R_r^2 + X_r^2} - V_j \frac{R_{fi}\sin\theta_j - X_{fi}\cos\theta_j}{R_{fi}^2 + X_{fi}^2} \tag{7}$$

$$\left[\Delta_a; \Delta_r\right] = \left[I^a_{calc} - I^a_{ref}; I^r_{calc} - I^r_{ref}\right] \tag{8}$$

Where: $\Psi = (V_k \cos\theta_k - V_j \cos\theta_j)$, $\Phi = (V_k \sin\theta_k - V_j \sin\theta_j)$.

B. Compliance with converter's current limit

The presented Newton-Raphson adaptation provides the grid steady-state conditions given the specified I^a_{ref} and I^r_{ref}. Based on the magnitude of the WTG's residual voltage, (1) calculates the expected I^+_r. If the quantified I^+_r is greater than or equal

to $I^+_{r,lim}$, then the converter could technically inject more than $I^+_{r,lim}$. However, the limit is imposed and an injection equal to $I^+_{r,lim}$ takes place. At this stage, since the proposed approach utilizes $I^+_{r,lim}$ as the initial guess, the grid conditions during the fault steady state have been estimated. If the calculated I^+_r is less than $I^+_{r,lim}$, the sought operational state is impracticable, and a more realistic estimation of the current must be done. This subsection presents an iterative approach capable of effectively handling such situations.

For specified I^a_{ref} and I^r_{ref} currents, suppose a WTG residual voltage V^+_{res} is obtained so that, once plugged into (1), yields a converter current $I^+_r < I^r_{ref}$. Then, there is an error/mismatch E, (9), that should be nullified. To do so, again a Newton-Raphson approach is used. Equation (10) describes the required derivative of E with respect to I^r_{ref}.

$$E = I^+_r - I^r_{ref} \tag{9}$$

$$\frac{dE}{dI^r_{ref}} = \frac{dI^+_r}{dI^r_{ref}} - 1 \tag{10}$$

Regarding dI^+_r/dI^r_{ref}, note in (1) that V_C, D_{band}, and $I^+_{r,pf}$ are constants, which imply null derivatives. The derivative of V^+_{res} is a function of I^r_{ref} that comes from the power flow computation. In other words, it is not an algebraic expression. Hence, its derivative is approximated by applying the fundamental definition of a derivative, (11). The $f(x)$ term relates to the V^+_{res} calculation given I^r_{ref}, i.e., it is the residual voltage magnitude already calculated by the approach of the previous subsection. To compute $f(x-h)$, one needs to run the adapted Newton-Raphson once again by inserting $I^r_{ref} - h$ as the specified reactive current, with h being a small value compared to the order of magnitude of the variables. Then, (11) will provide a $d|V^+_{res}|/dI^r_{ref}$ estimation that enables the calculation of dE/dI^r_{ref}, as in (12).

$$\frac{df}{dx} = lim_{h\to 0}\frac{f(x) - f(x-h)}{h} \tag{11}$$

$$\frac{dE}{dI^r_{ref}} = -K_{factor}\frac{d|V^+_{res}|}{dI^r_{ref}} - 1 = E' \tag{12}$$

Once E' has been estimated, the following steps take place: (i) obtain the next specified ($I^{r,next}_{ref}$) for the converter reactive current by following (13); (ii) (4) yields $I^{a,next}_{ref}$; (iii) apply $I^{r,next}_{ref}$ to the adapted Newton-Rhapson during the fault; (iv) plug the new residual voltage at the WTG into (6) and extract I^+_r; (v) verify the mismatch E; (vi) repeat the process until $|E|$ is less than or equal to a small user-defined tolerance. Upon convergence of the iterative process, one obtains a specified converter current related to a residual WTG voltage that is feasible regarding (1). Hence, this is a more realistic estimation of the short-circuit contribution of type IV WTGs.

$$I^{r,next}_{ref} = I^r_{ref} - E/E' \tag{13}$$

Fig. 5 presents a flowchart of the analytical approach. By the end of the process, the method provides the estimated active and reactive currents that the WTG will inject during the steady state of the three-phase fault.

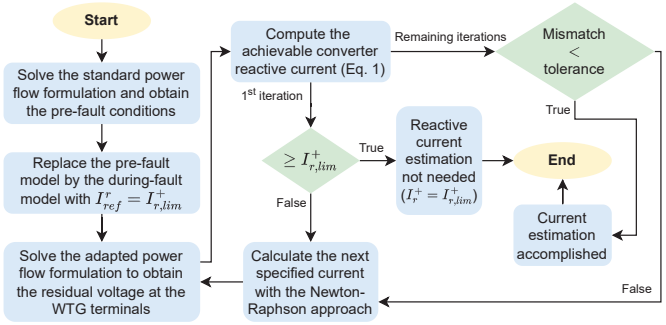

Fig. 5. Flowchart of the steady-state current analytical estimation.

C. Simulation setup and results

To assess the proposed analytical method, 48 base cases (BSs) of three-phase faults from the field-validated EMT model were utilized. For all cases, K_{factor} and the WTG pre-fault active power reference (P_{ref}) are equal to 2 and 1, respectively. Table I provides additional input data, where V_{ref}, V_r, and SCR are the WTG pre-fault voltage reference, the retained voltage at the fault point, and the short-circuit ratio, respectively. Each of the base cases was subjected to the two grid codes described in Section III, thus yielding 96 different simulations regarding the steady-state studies. Equations (14) and (15) quantify the fault impedance. The addressed cases relate to diverse during-fault scenarios in which $|V^+_{res}|$ often implies reactive injections that are less than $I^+_{r,lim}$, hence requiring accurate estimations.

TABLE I
INPUTS FOR ANALYTICAL SIMULATIONS

BS	V_{ref}	SCR	$\frac{X}{R}$	V_r	f_{loc}	BS	V_{ref}	SCR	$\frac{X}{R}$	V_r	f_{loc}
1	1	15	7	0.2	0.01	**25**	1.08	15	7	0.25	0.5
2	1	10	7	0.2	0.01	**26**	1.08	10	7	0.25	0.5
3	1	7	7	0.2	0.01	**27**	0.95	7	7	0.25	0.5
4	1	5	7	0.2	0.01	**28**	0.95	5	7	0.25	0.5
5	1	15	15	0.4	0.01	**29**	1.08	15	15	0.45	0.5
6	1	10	15	0.4	0.01	**30**	1.08	10	15	0.45	0.5
7	1	7	15	0.4	0.01	**31**	0.95	7	15	0.45	0.5
8	1	5	15	0.4	0.01	**32**	0.95	5	15	0.45	0.5
9	1.08	15	7	0.2	0.01	**33**	1	15	7	0.3	0.9
10	1.08	10	7	0.2	0.01	**34**	1	10	7	0.3	0.9
11	0.95	7	7	0.2	0.01	**35**	1	7	7	0.3	0.9
12	0.95	5	7	0.2	0.01	**36**	1	5	7	0.3	0.9
13	1.08	15	15	0.4	0.01	**37**	1	15	15	0.5	0.9
14	1.08	10	15	0.4	0.01	**38**	1	10	15	0.5	0.9
15	0.95	7	15	0.4	0.01	**39**	1	7	15	0.5	0.9
16	0.95	5	15	0.4	0.01	**40**	1	5	15	0.5	0.9
17	1	15	7	0.25	0.5	**41**	1.08	15	7	0.3	0.9
18	1	10	7	0.25	0.5	**42**	1.08	10	7	0.3	0.9
19	1	7	7	0.25	0.5	**43**	0.95	7	7	0.3	0.9
20	1	5	7	0.25	0.5	**44**	0.95	5	7	0.3	0.9
21	1	15	15	0.45	0.5	**45**	1.08	15	15	0.5	0.9
22	1	10	15	0.45	0.5	**46**	1.08	10	15	0.5	0.9
23	1	7	15	0.45	0.5	**47**	0.95	7	15	0.5	0.9
24	1	5	15	0.45	0.5	**48**	0.95	5	15	0.5	0.9

$$Z_{fa} = \frac{V_r \cdot Z_{th}}{1 - V_r} \cdot (1 - f_{loc}) \tag{14}$$

$$R_{fa} = \sqrt{\frac{(Z_{fa})^2}{1 + (X/R)^2}} \ , \ X_{fa} = \sqrt{(Z_{fa})^2 - (R_{fa})^2} \tag{15}$$

The presented cases were subjected to the approaches from subsections III-A and III-B. The following simulation aspects are highlighted: (i) although the WTG could technically inject more than 1 p.u. of reactive current in some cases, the control strategy for the studied system applies an injection limit ($I^+_{r,lim}$) of 1 p.u., so that a meaningful active current injection can occur, as discussed in [3]. Thus, for these cases, the analytical approach keeps the reactive injection at 1 p.u.; (ii) the maximum during-fault current magnitude (I_{max}), (4), of the converter under analysis is equal to 1.11 p.u.; (iii) for all cases, $I^r_{ref} = 1$ p.u. is the reactive current initial guess. Fig. 6 presents the obtained current components and residual voltages for different fault conditions, given by Table I, during the steady-state of the three-phase faults compared to PSCAD. As seen, the proposed analytical approach effectively quantified the current injected by the WTG during the faults.

Table II provides the mean relative errors (MRE) given all 96 cases, with 48 corresponding to GC 1 and 48 to GC 2. The results indicate that the proposed approach can accurately estimate the steady-state SCC contributions of type IV WTGs. The EMT simulations apply the faults for 500 ms and the results used for comparison (i.e., PSCAD results in Fig. 6) are given by the average of the last 350 ms of the fault. Therefore, small deviations compared to the analytical approach were expected since faults in EMT simulations may not always reach perfect steady-state.

TABLE II
MEAN RELATIVE ERRORS OF THE ANALYTICALLY ESTIMATED QUANTITIES PER GRID CODE, IN %

	MRE - $\lvert V^+_{res}\rvert$	MRE - I^+_r	MRE - I^+_a
GC1	0.69	0.46	0.72
GC2	0.76	1.20	1.09

As a final remark, it is emphasized that more validation was performed to ensure the methodology works. Cases with diverse fault locations, X/R ratio, etc, were simulated and yielded the same accuracy level presented in Table II. However, for conciseness, such cases aware not shown in this paper.

IV. TRANSIENT CURRENTS ML-BASED ESTIMATION

Estimating the currents during the transient stages of the fault is as crucial as addressing the estimation of the currents during the steady state. Therefore, this section will address how some of the currents can be estimated during the highly complex transient period at the inception of the fault. The novel methodology uses machine-learning (ML) algorithms and comprises a combination of pre-validated EMT models and steady-state estimated currents. It can either be used together with the solution from Section III or as a standalone tool coupled to other types of SCC steady-state estimation.

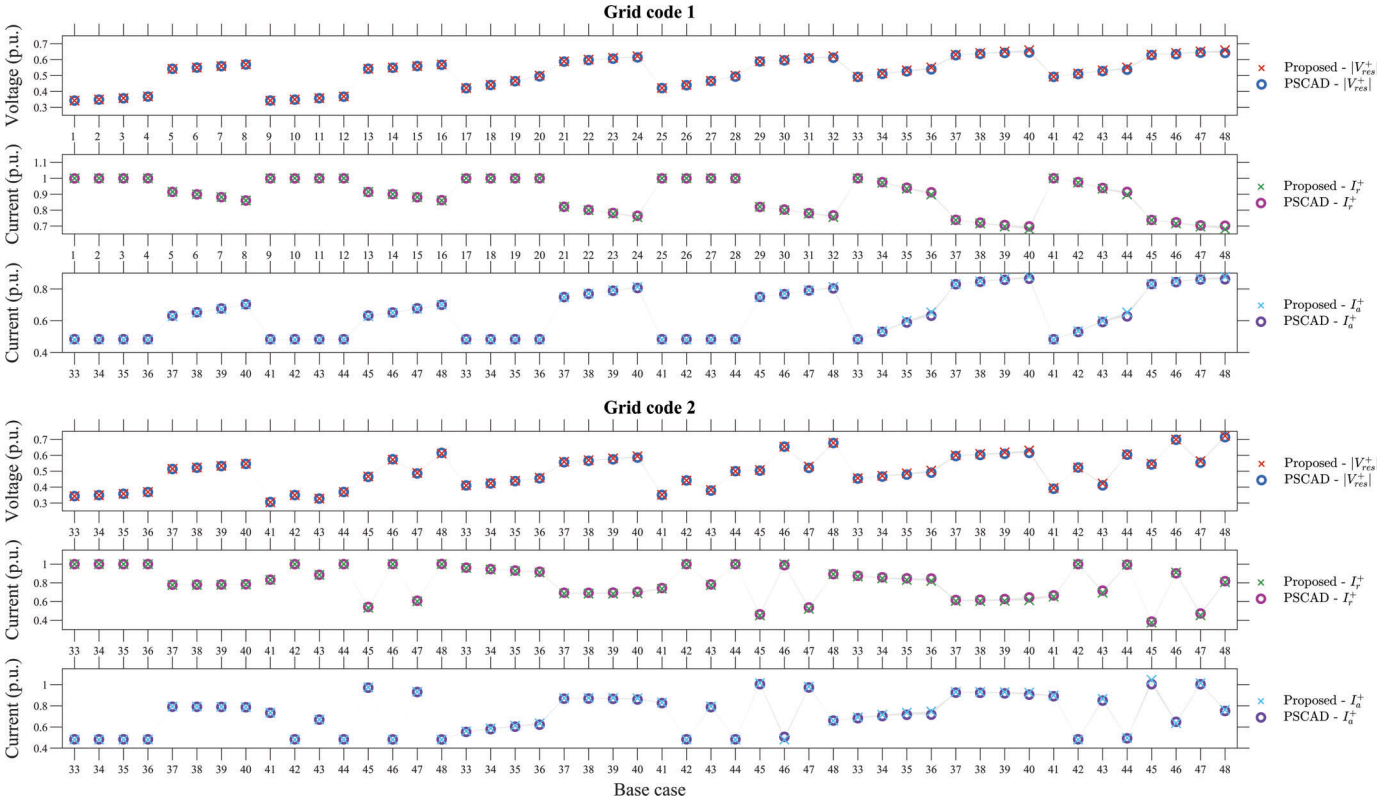

Fig. 6. Analytical estimation of steady-state quantities, in p.u., for different fault conditions.

The justification for using ML comes from the fact that the analytical representation of the peak current is not straightforward, especially in industrial controls where the level of complexity is very high and ever-changing. During the transient, factors such as control communication delays, transducers, control bandwidths, power electronics hardware, and other inherited parameters, play a crucial role in the response of the turbine besides the traditional network conditions and parameters. Three main shortcomings come into play when modeling such phenomena analytically:

1) Among different manufacturers, there is a wide variety of implementations of controls and all the other side hardware and modulation.
2) For generic implementations, to the knowledge of the authors, the industry has not yet found a way to model this phenomenon realistically.
3) Even if some complex analytical representation is found, it would most likely require a white-box representation of many of the control parts, not respecting the protection of intellectual property. The representation via ML models can be performed in a black-box manner, respecting the intellectual property of the manufacturer while presenting results with good accuracy.

This section uses more than 16000 cases with the validated EMT models incorporating variations of the parameters, fault conditions, operating points, and grid codes, as shown in Table III. In these simulations, I_{prio} is used for defining two different types of reactive current priority during the fault, i.e. only positive sequence or both positive and negative sequence. The methodology was mainly applied to a randomly selected subset of the data of around 8000 cases (50%).

TABLE III
PARAMETERS AND RANGES USED IN SIMULATIONS

Parameters	Range	Parameters	Range
V_{ref}	0.92 - 1.08 p.u	I_{prio}	Q - Pos or PosNeg
X/R	2 - 13	f_{loc}	0 - 1
SCR	1.5 - 10	K_{factor}	2 - 3.5
P_{ref}	0.25 - 1 p.u	V_r	0 - 0.8

By leveraging these validated models and using their results to train the ML models, the estimation of the transient currents can be used to study short-circuit currents in large systems whilst maintaining computational efforts low. Below are the main inputs (X_{ML}) and outputs (y_{ML}) of the ML models trained for estimating the currents. There are four classes of inputs: pre-fault operating points; fault steady-state estimated operating points; impedance to the fault and fault conditions; FRT grid code parameters; and peak current hardware limit.

$$X_{ML} = \begin{cases} I^{+}_{act,pre},\ I^{+}_{react,pre}\ , V^{+}_{pre}; \\ I^{+}_{act,ss},\ I^{+}_{react,ss},\ V^{+}_{ss},\ I^{-}_{react,ss},\ V^{-}_{ss}; \\ R_{wtg-f}, X_{wtg-f},\ F_{type},\ R_{fault},\ X_{fault},\ F_{angle}; \\ K^{+}_{factor},\ K^{-}_{factor},\ Seq^{+-}_{prio},\ V_{prio},\ I_{peak-lim}; \end{cases}$$

Outputs can be separated into three classes: peak quantities of the instantaneous current waveforms (I_{pk}); maximum quantities in the sequence components (I^{+}_{max} & I^{-}_{max}); and maximum quantities at each odd cycle from the first to the fifth ($I^{+/-}_{1st}$, $I^{+/-}_{3rd}$ & $I^{+/-}_{5th}$).

$$y_{ML} = \begin{cases} I_{pk} \\ I^{+}_{max}; I^{-}_{max} \\ I^{+}_{1st-cyc}; I^{+}_{3rd-cyc}, I^{+}_{5th-cyc} \\ I^{-}_{1st-cyc}; I^{-}_{3rd-cyc}, I^{-}_{5th-cyc} \end{cases}$$

The next subsections show different use-cases and estimations using various ML models. Each model has been optimized for its hyper-parameters. The algorithms were optimized using GridSearch algorithm from the hypopt package, which performs hyper-parameter optimization using a testing set.

A. Peak Current Estimation in the Sub-transient Stage

In Fig. 7 the three different models, Light Gradient Boosting Machine (LGBM), Random Forest (RF), and Multi-Layer Perceptron (MLP), are compared for their performance of predicting the peak current (I_{pk}). The y-axis shows the % of the total testing data set. The x-axis introduces four categories, meaning the percentage of variation of the estimated result against the validated EMT model. Initially, the comparison between algorithms is made using only 843 simulations (i.e. 5% of the data) for training the ML model, whereas the remaining 95% of the data was used for testing, as shown in Fig. 7. In conclusion, LGBM and RF perform relatively better than MLP. However, the three models perform well, in general, for a very low amount of training data.

Due to its rapidness in training and optimizing hyperparameters, LGBM was chosen to be further explored in Fig. 8, which provides a comparison between using 5% and 50% for training data. The plots show the result of the estimation on the testing dataset (i.e. 95% and 50%, respectively). Graphically, it can be seen that the model behaves much better when a

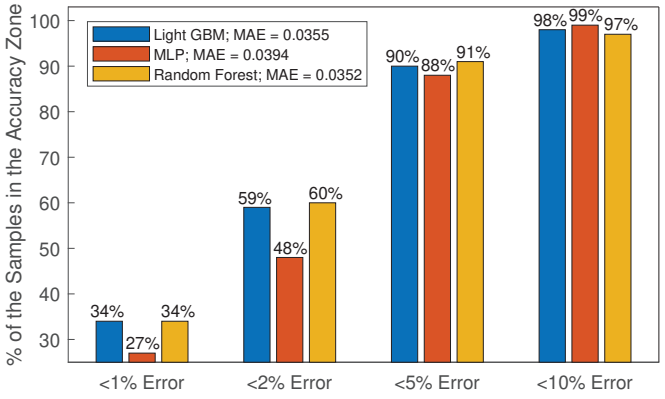

Fig. 7. Comparison of different regression algorithms for predicting peak current using 5% of the data.

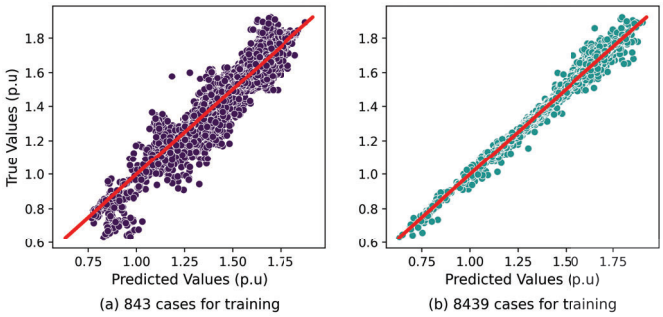

Fig. 8. Comparison of different regression algorithms to predict peak current on the testing dataset using 843 cases (5%) and 8439 (50%) of the data.

larger portion of the data is utilized for training. The hyperparameters of the optimized model were *learning rate = 0.08, number of estimators = 2000, and maximum depth = 20.* In this case, the model of sub-figure (b) had 87.45% and 98.55% of the test cases below 2% and 5% relative error, respectively.

Fig. 9 shows a feature importance analysis. As seen, the top features are a combination of pre-fault and fault steady-state (estimated) inputs together with fault conditions imposed on the turbine. The most important is the pre-fault active current, which dictates the majority of the total pre-fault injected current. The fault impedance is also crucial, as it highly influences how much the current can rise before the converter starts controlling it after a few milliseconds. As shown in analytical and statistical studies from [3], FRT-related parameters play a small role during the early transient stages as the converter has not yet switched to FRT mode.

B. Prediction of Other Quantities during the Transient Stage

Following the prediction of the peak current, it is also of interest to estimate the values of other transient quantities. Fig. 10 presents estimations for other eight different currents.

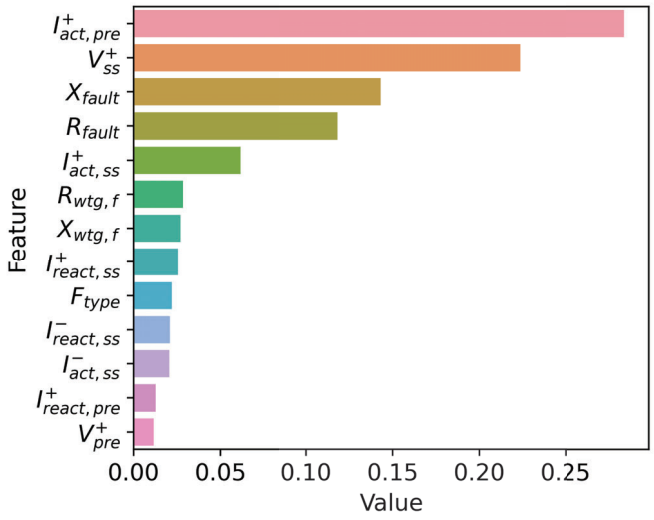

Fig. 9. Overall importance of the features for predicting peak current using RF/LGBM - Only features with $>$ 0.01 importance.

One LGBM ML model was used for each estimation and the hyperparameters were once more optimized for each quantity estimated. Each of the models utilizes 50% of the total data set for training and the remaining 50% for testing the data, which are shown in the figure. Results show that the estimation is still quite accurate even in light of the nonlinearities of the transient stage in the third and fifth cycles.

C. On the Accuracy and Practicality of ML-Based Short-Circuit Studies

In practical studies, implementing the ML methodology may pose challenges, particularly due to the potentially high number of simulations needed to train the model. Nevertheless, it's

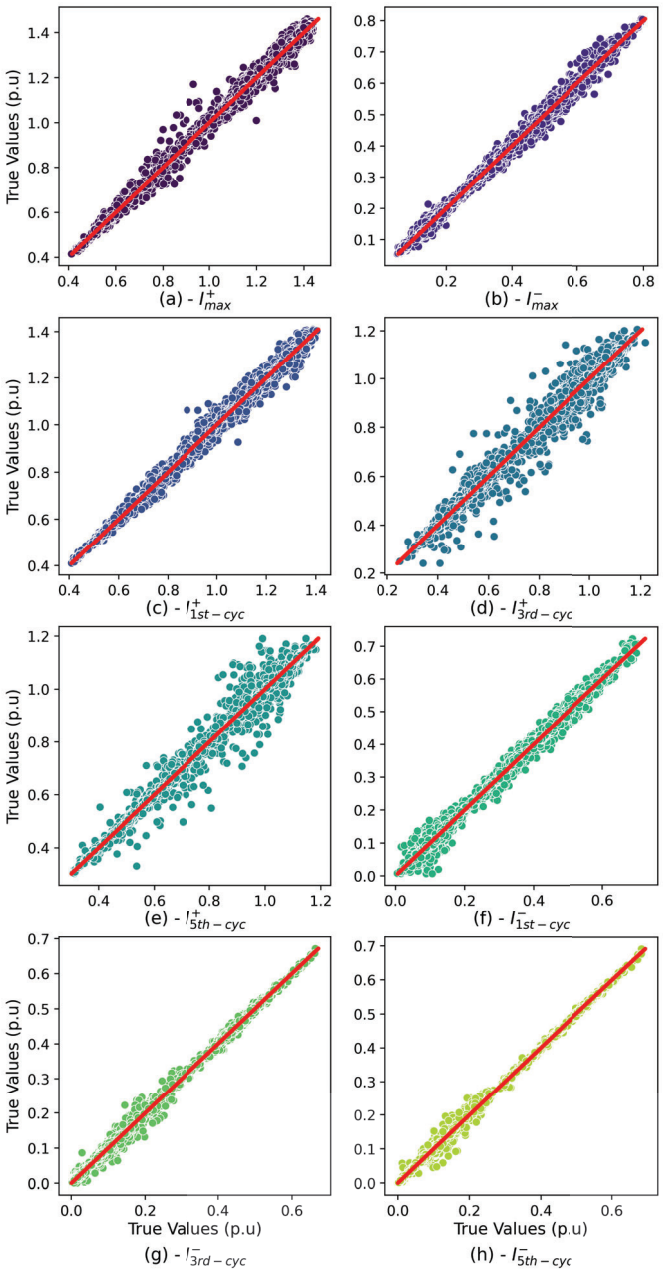

Fig. 10. Magnitude predictions for other values of transient currents.

important to note that unlike detailed EMT studies demanding high accuracy, short-circuit studies can tolerate lower levels of precision. Often, parameters such as impedances used in short-circuit studies for conventional generation have high tolerances, yielding less precise results.

In this context, once an acceptable level of accuracy is established, the number of simulations required in the paper could technically be reduced. For future research, exploring new techniques for estimating transient currents is imperative. This will enable the industry to reach a consensus on the usability and desired levels of accuracy for different techniques.

V. Conclusions

This paper proposes two novel methods that are jointly used to estimate the current contributions at the transient and steady-state stages of a fault. The methods provide a new level of transparency on the SCC response of type IV WTGs. To validate the methodologies, field-validated EMT models with the embedded control source code as *.dlls* have been used.

For the steady state, an analytical estimation method considers different grid codes, operating conditions, and fault scenarios. Initially, a power flow algorithm obtains the pre-fault operating conditions. Then, a Newton-Rapshon approach iteratively estimates the steady-state positive sequence current contributions for balanced faults. The method achieves very accurate results with mean absolute errors of no more than 1.21% compared to PSCAD.

In parallel, by using field-validated EMT simulations, a machine learning-based approach estimates the maximum peak current during faults. The trained machine learning model is coupled to the analytical method and utilizes the estimated steady-state currents to improve the prediction of the peak currents. The results show that most of the estimated currents are below 5% of error and can be used for short-circuit studies.

In future studies, the methods will be extended in three different directions: 1) The steady-state methodology will be extended to cover unbalanced faults; 2) The fault-clearing stage of the turbine will also be investigated; 3) A systematic software will be done to incorporate the methodologies deployed here; 4) Evaluate the feasibility of application commercial of the ML method for transient estimation; and 5) Coordination with standardization working groups (e.g. IEC 60909-0) to bring these new methodologies of estimation so that supply of information is more harmonized for original equipment manufacturers (OEMs).

References

[1] I. Kasikci, *Short circuits in power systems : a practical guide to IEC 60909-0*. Wiley-VCH, 2018.

[2] IEC, "IEC 60909 short-circuit currents in three-phase a.c. systems - Part 0: Calculation of currents," 2016.

[3] G. M. Gomes Guerreiro, R. Sharma, F. Martin, P. Ghimire, and G. Yang, "Concerning short-circuit current contribution challenges of large-scale full-converter based wind power plants," *IEEE Access*, pp. 1–19, 2023.

[4] L. Thurner and M. Braun, "Vectorized Calculation of Short Circuit Currents Considering Distributed Generation - An Open Source Implementation of IEC 60909," in *2018 IEEE PES Innovative Smart Grid Technologies Conference Europe (ISGT-Europe)*. IEEE, 2018, pp. 1–6.

[5] J. Jia, G. Yang, and A. H. Nielsen, "Fault Analysis Method Considering Dual-Sequence Current Control of VSCs under Unbalanced Faults," *Energies*, vol. 11, no. 7, 2018.

[6] T. Kauffmann, U. Karaagac, I. Kocar, S. Jensen, E. Farantatos, A. Haddadi, and J. Mahseredjian, "Short-Circuit Model for Type-IV Wind Turbine Generators With Decoupled Sequence Control," *IEEE Transactions on Power Delivery*, vol. 34, no. 5, pp. 1998–2007, 10 2019.

[7] L. V. Strezoski, B. Dumnic, B. Popadic, M. Prica, and K. A. Loparo, "Novel fault models for electronically coupled distributed energy resources and their laboratory validation," *IEEE Transactions on Power Systems*, vol. 35, no. 2, pp. 1209–1217, 2019.

[8] F. Jimenez-Buendia, A. Honrubia-Escribano, A. Lorenzo-Bonache, E. Artigao, and E. Gomez-Lazaro, "Short-Circuit Current Contribution of Doubly-Fed Wind Turbines According to IEC and IEEE Standards," *IEEE Transactions on Power Delivery*, vol. 36, no. 5, pp. 2904–2912, 10 2021.

[9] IEC, "IEC 61400-21 wind energy generation systems - Part 21-1: Measurement and assessment of electrical characteristics - Wind turbines," 2019.

[10] G. M. G. Guerreiro, F. Martin, G. Yang, and B. Andresen, "New Pathways to Future Grid Compliance for Wind Power Plants," *21st Wind & Solar Integration Conference, The Hague, Netherlands - IET Conference Proceedings*, pp. 115–121(6), October 2022.

[11] E.ON Netz GmbH, *Grid Code-High and Extra High Voltage*, Bayreuth, April 2006.

[12] "Ordinance on system services by wind energy plants (SDLWindV)," Verordnung zu Systemdienstleistungen durch Windenergieanlagen, 2009, last amended by Article 10 of the law from October 13, 2016.

Acknowledgments and Legal Disclaimer

The authors would like to acknowledge the support of Siemens Gamesa Renewable Energy (SGRE) and InnoCyPES (Innovative tools for cyber-physical energy systems), where three of the co-authors have received funding from the European Union's Horizon 2020 research and innovation programme under the Marie Sklodowska Curie grant agreement No 956433. Figures and values presented in this paper should not be used to judge the performance of Siemens Gamesa Renewable Energy technology as they are solely presented for demonstration purposes. Any opinions or analyses contained in this paper are the opinions of the authors and are not necessarily the same as those of Siemens Gamesa Renewable Energy.